Structural Dynamics of Strongly Segregated Block Copolymer Electrolytes

Onyekachi Oparaji,[a,b] Suresh Narayanan,[c] Alec Sandy,[c] Subramanian Ramakrishnan,[a,b] and Daniel Hallinan Jr.[a,b,*]

[a]*FAMU-FSU College of Engineering, Florida A&M University-Florida State University, Tallahassee, Florida 32310, USA*

[b]*The National High Magnetic Field Laboratory, Florida State University, Tallahassee, Florida 32303, USA*

[c]*Argonne National Laboratory, Argonne, Illinois 60439, United States*

*Corresponding author, dhallinan@fsu.edu, 850-645-0131

Abstract

Polymer electrolytes are promising materials for high energy density rechargeable batteries. However, they have low ion transport rates and gradually lose electrode adhesion during cycling. These effects are dependent on polymer structure and dynamics. This motivates an investigation of diblock copolymer electrolyte dynamics. Structural and stress relaxations have been measured with x-ray photon correlation spectroscopy (XPCS) and rheology, respectively, as a function of salt concentration and temperature. The polymer electrolyte studied in this work is a mixture of poly(styrene-b-ethylene oxide), SEO, and lithium bis-trifluoromethanesulfonimide, LiTFSI. Results from XPCS experiments showed hyperdiffusive motion for various lithium salt concentrations and at varying temperatures, which is indicative of soft glassy materials. This behavior is attributed to cooperative dynamics. The decay time was a weak, non-monotonic function of salt concentration and decreased with increasing temperature, in an Arrhenius fashion. In contrast, the shear modulus decreased with increasing salt concentration and increasing temperature. The entanglement relaxation from rheological measurements followed Vogel-Fulcher-Tammann behavior. The structural decay time was slower than the entanglement relaxation time at temperatures above the glass transition temperature, but they were approximately equal at T_g regardless of salt concentration. This may indicate a fundamental connection between cooperative structural motion and polymer chain motion in this material.

1.0 Introduction

Advanced energy storage is integral to transitioning to a sustainable energy society. The most advanced batteries currently available on the market are lithium-ion batteries, which offer the highest energy density of any commercial battery. Safety continues to be the greatest concern for lithium-ion batteries that contain volatile, flammable organic solvent electrolytes.[1] This is particularly true for electric vehicles that contain large amounts of energy that would be violently released during a catastrophic failure. For example, the Tesla Roadster contains thousands of 18650 batteries[2]. On the other hand, electric vehicles leverage our transition to a sustainable energy infrastructure by replacing fossil fuel consuming vehicles with those that utilize renewable energy sources. Safe, long-lasting batteries with high power and high energy density would enable an expansion of the electric vehicle market by increasing driving range and decreasing vehicle cost.

Polymer electrolytes are an inherently safe alternative to organic solvent electrolytes.[3] Nanostructured polymer electrolytes, such as block copolymers and polymer nanocomposites, are compatible with electrodes, such as lithium metal, that have a theoretical capacity nearly ten times that of graphite electrodes used in commercial lithium-ion batteries.[4, 5] A glassy or inorganic phase provides mechanical strength, while a soft polar phase allows for ionic conduction. Low ionic conductivity is the major impediment to adoption of polymer electrolyte in lithium metal batteries as distinct from lithium-ion batteries.

Ionic conductivity is a function of ion concentration and mobility. In dry polymer electrolytes, such as poly(ethylene oxide) (PEO) and a lithium salt, ion mobility is coupled to segmental relaxation of the polymer.[6] The incorporation of lithium salt into PEO increases the glass transition temperature.[7] In other words, the segmental relaxation of the polymer is slowed by

coordination with Li^+ ions (on average six ether units are involved in the lowest energy state).[8, 9] From the free-volume perspective this implies that dissolution of salt in PEO causes a decrease in fractional free volume.[10, 11] The configurational entropy of the system is probably a more appropriate perspective. From this perspective, ion coordination increases the minimum size of a "'cooperatively rearranging' region" of PEO.[12, 13] So, ion and polymer mobility are coupled as well as being composition dependent.

Recent reports have investigated the role of ordered block copolymer grain size on ionic conductivity. Conductivity was inexplicably found to decrease with increasing grain size.[14] The authors postulated that perhaps ion dynamics is faster in grain boundaries than within the ordered phase. Block copolymer electrolyte conductivity was found to increase with the incorporation of nanoparticles that can drive morphological phase transitions[15] or stabilize grain boundaries[16]. Although grain size only plays a minor role in the macroscopic mechanical properties of block copolymers,[17] it appears to play a significant role in the ionic conductivity of block copolymer electrolytes. Furthermore, the effect of salt concentration on the mechanical properties of block copolymer electrolytes has not been systematically investigated. Thus, it is of interest to measure dynamics of block copolymer electrolytes of known grain size and salt concentration. In addition to examining chain dynamics with rheology, grain dynamics can be examined using x-ray photon correlation spectroscopy (XPCS).

XPCS is a powerful technique for investigating the dynamics of nanostructured materials. In the same way that dynamic light scattering can be used to measure the diffusion of polymers and colloids in solution, XPCS can be used to measure dynamics in materials with electron density contrast (i.e. structure) on time scales between 10^{-4} and 10^4 s, and as fast as 50 ns has been achieved.[18] The advantage of XPCS over light scattering techniques is that it can be used with

optically opaque samples.[19] Diffusing wave spectroscopy can use multiple light scattering on turbid samples but cannot be applied to opaque samples.[20] The most powerful aspect of XPCS is that it can access a much broader range of length scales including atomic[21, 22] (light scattering is limited to structures larger than about 100 nm)[23]. There are some reports of using XPCS to measure dynamics in disordered and weakly ordered block copolymers (BCPs),[24-30] but no investigations of strongly segregated BCPs with XPCS. Since static x-ray scattering is necessarily collected (through time) the nanostructure of the material is simultaneously monitored during measurements of dynamics.

Lithium bis-trifluoromethanesulfonimide (LiTFSI) is the best performing lithium salt in PEO-based electrolytes, i.e. this polymer electrolyte has the highest ionic conductivity. The salt also affects the structure of poly(styrene-*b*-ethylene oxide), SEO, block copolymers. LiTFSI increases the strength of segregation and swells the BCP domains.[31, 32] However, with increasing salt concentration the long-range order of the BCP decreases for a given annealing time,[33] perhaps due to the stronger segregation strength, i.e. higher order-disorder transition temperature, T_{ODT}. This suggests that the salt slows grain dynamics.

Motivated by these findings, we present the effect of lithium salt concentration on polymer dynamics by measuring both the structural and stress relaxation behavior using XPCS and rheology, respectively. Since rheological properties are sensitive to deformation history, samples are thermally annealed before conducting small-amplitude oscillatory shear rheology and XPCS. The BCP is a strongly segregated lamellar SEO. Within a temperature range of 100 and 180 °C, the effect of LiTFSI salt concentration was investigated based on the segmental, entanglement and structural relaxation processes of the electrolyte melt. The relationship between these

polymer relaxations and ion concentration give insight into the design of the next generation of polymer electrolytes for lithium batteries.

2.0 Experimental

2.1 Materials

SEO used in this study was anionically synthesized, purified, and characterized using methods described previously.[34] The SEO copolymer comprises a polystyrene block (M_N = 133 kg/mol, M_W = 145 kg/mol) and PEO block (M_N = 114 kg/mol). The polydispersity index (PDI) of the SEO was measured as 1.11 using gel permeation chromatography (Viscotek GPCmax with dimethylformamide (DMF) solvent and 0.05 wt% LiBr). The PEO volume fraction is 0.42 as measured through ^{1}H nuclear magnetic resonance (NMR) spectroscopy and calculated using the density of each block at 25 °C.[35]

SEO electrolyte membranes were prepared by solution casting from n-methyl-2-pyrrolidone according to a procedure described previously.[36] Each SEO electrolyte (SEO-LiTFSI) membrane consists of SEO copolymer and bis(trifluoromethane)sulfonimide lithium salt $LiN(SO_2CF_3)_2$. The concentration of the lithium salt is expressed in term of the stoichiometric proportion (r = $[Li^+]/[EO]$) of lithium cations from the salt to ethylene oxide monomers of the polymer.

2.2 SAXS and XPCS

Small angle x-ray scattering (SAXS) and x-ray photon correlation spectroscopy (XPCS) were used to investigate the nature of the electron density contrast in SEO-LiTFSI systems from the static and dynamic point of view, respectively. Samples were prepared by melt pressing the SEO-LiTFSI electrolyte into stainless steel spacers sealed in an argon environment with H_2O and

O_2 less than 0.1 ppm using custom sample holders with Kapton windows. All samples were annealed at 180 °C for 2 days.

SAXS measurements were performed at beamline 8-ID-I at the Advanced Photon Source (APS), Argonne National Laboratory, in a temperature interval between 100 and 180 °C. The x-ray energy was set at 10.86 keV (0.1142 nm). The sample-to-detector distance for all measurements was 4 m. The SAXS images were azimuthally averaged to produce profiles of intensity, I, versus wavevector, $q = 4\pi \sin(\theta/2)/\lambda_{x\text{-}ray}$, where $\lambda_{x\text{-}ray}$ is the x-ray wavelength and θ is the scattering angle.

XPCS measurements were performed in the same beamline (8-ID-I). Details of the beamline optics and principle of operation have been reported elsewhere.[37] All measurements were conducted using coherent x-rays. To minimize any possible effects of x-ray sample damage or beam heating, for each data acquisition sequence, the sample position was adjusted to illuminate a fresh spot on the sample. NMR analysis conducted on the SEO samples before and after exposure to x-rays ensured that no detectable sample damaged occurred. As shown in Figure S1, the normalized NMR spectra of both the ethylene oxide and styrene protons show no change in chemical shift after exposure to x-rays. In addition, the mole fraction of PEO (0.33) was the same before and after thermal annealing and exposure to x-rays. As shown in Figure S2, the GPC traces of the refractive index (RI) detector show no significant different between the as-synthesized neat polymer and the polymer (r = 0.02 mol_{Li+}/mol_{EO}) exposed to x-rays during XPCS experiments. The average scattering intensity was constant during the collection of XPCS data, which is another indication that no significant beam damage occurred.

Electron density gradients cause a speckle pattern in the instantaneous x-ray scattering profile. Over time the gradients and therefore speckle patterns change causing the normalized intensity autocorrelation function, g_2, to decay to a value of one at long time.

$$g_2(q,t) = \frac{\langle I(q,t_1) I(q,t_1+t) \rangle}{\langle I(q,t_1) \rangle^2} \quad (1)$$

The angle brackets denote an average over t_1.[23] $g_2(q,t)$ can be related to the field correlation function, $g_1(q,t)$, using the Siergert equation.[38]

$$g_2(q,t) = 1 + |g_1(q,t)|^2 \quad (2)$$

And $g_1(q,t)$ can be modeled using a Kohlrausch-Williams-Watts (KWW) function [39].

$$g_1(q,t) = A e^{-[t/\tau(q)]^\beta} \quad (3)$$

The initial value of A is related to the speckle contrast of the experimental set-up that was calibrated using the speckle pattern of an immobile aerogel. The KWW function assumes a single relaxation time, τ, that is stretched or compressed by β. Combining equations 2 and 3,

$$g_2(q,t) = 1 + A e^{-2[t/\tau(q)]^\beta} \quad (4)$$

The KWW exponent (β) can be used to define a stretched system (β < 1) or compressed system when β > 1. A parametric investigation of the impact of β on g_2 is presented in Figure S3.

XPCS measures the characteristic relaxation(s) by fitting the KWW function (equation 4) to the g_2 measured experimentally. In these regressions, A, β, τ, and the baseline (shown as 1 in equation 4) can be adjustable parameters. Regressions were conducted with and without the baseline fixed to 1. A fixed baseline significantly decreased the uncertainty of experiments at 100 °C, but had no effect on results at other temperatures. β and τ values at 100 °C are reported for fixed baseline regressions. The relaxation time(s) determined by XPCS can be attributed to different physical phenomena that depend on the system studied. We use the term “relaxation” in

a general sense to refer to the decay time of the autocorrelation function. This does not imply that it is ergodic. In fact, one of the advantages of XPCS is its evaluation of dynamics in non-equilibrium systems.[19] Any system with grains of finite size is not in its lowest energy state. Therefore, strongly segregated BCPs and even BCPs quenched well below T_{ODT} have a metastable grain structure.[40] In our annealed samples the evolution of grain structure is on the order of days, which is slow compared to the time scale of XPCS measurements on the order of seconds. Thus, XPCS takes a snapshot of structural motion for a given grain structure.

2.3 Rheology

The SEO electrolytes for rheological testing were molded using a hot press at 3000 psi and 120 °C. Each sample was pressed into discs of 8 mm in diameter and 1 ± 0.1 mm thickness in a dry room of relative humidity ~ 0.5 %RH (-55 °C dew point). The discs were annealed overnight at 120 °C under vacuum. A high precision Anton Paar stress-controlled rheometer was used with parallel-plate geometry for the dynamic measurements in the angular frequency range 0.01 – 100 rad/s at low strain amplitude (γ = 1%), and torque controlled within 1.25 x 10^4 to 1.85 x 10^4 μNm. For each set of experiments, samples were carefully transferred from a sealed glass vial into the dry-nitrogen-purged sample chamber of the rheometer in less than 30 seconds. This was followed by an hour thermal equilibration before each run. All measurements were conducted isothermally, at various temperatures between 100 °C and 180 °C. The temperatures were controlled to within 0.2 °C of the set points with a continuous purge of dry nitrogen gas. From the Williams, Landel, Ferry (WLF) time-temperature superposition principle, master curves were constructed for each sample at a reference temperature of 120 °C.

3.0 Results

3.1 Microstructure (SAXS)

The effect of salt concentration on the morphology of SEO-LiTFSI electrolytes was investigated from SAXS experiments as shown in Figure 1a. The SAXS patterns in Figure 1a are indicative of the lamellar morphology, which has been confirmed with AFM.[41] X-ray scattering from a lamellar morphology should produce a primary scattering peak, q^*, and integer multiples. In Figure 1a, scattering maxima q^*, $2q^*$, $3q^*$, and $4q^*$ are denoted by data symbols. Studies have shown that depending on the molecular weight of the block copolymer, the presence of salt causes the broadening of scattering peaks,[42] change in the morphology,[33, 43] as well as stabilization of the ordered phase.[44, 45] We report the SAXS profile of pure SEO membrane and SEO-LiTFSI electrolyte for different salt concentrations and temperatures. It is evident that, with the possible exception of r = 0.02 mol_{Li+}/mol_{EO}, the block copolymer has an ordered lamellar microstructure as indicated by the primary, secondary, tertiary, and quaternary peaks in the scattering profiles.

Figure 1b shows 1D SAXS profiles for r = 0.02 at 140 °C from the beginning and end of XPCS data collection. In all experiments, the total intensity was tracked during data collection and found to change by less than 5%. This is a strong indication of the absence of beam damage. The data sets in Figure 1b are the worst case scenario of all data included in this study. There is a 12% increase of intensity at the 2q* maximum over the course of the experiment, but very little change elsewhere. In order to ensure that the change at 2q* is not due to beam damage, a two time correlation of the data is reported in Figure S4. It shows that the decorrelation rate does not change over the course of the experiment, indicating that the measured dynamics are not due to beam damage. Corresponding two-dimensional scattering patterns are presented separately in

Figure S5 and overlaid in Figure S6 to show that the speckle patterns clearly change over the course of the experiment. The average 2D SAXS profile for this experiment is shown in Figure 1c. This study is focused on the wave vector range in which scattering from the BCP structure occurs. This is near the center of Figure 1c. In this region there are smooth intensity variations, i.e. lack of speckles in the averaged pattern, which indicates that the speckles move or decorrelate over the course of the experiment.

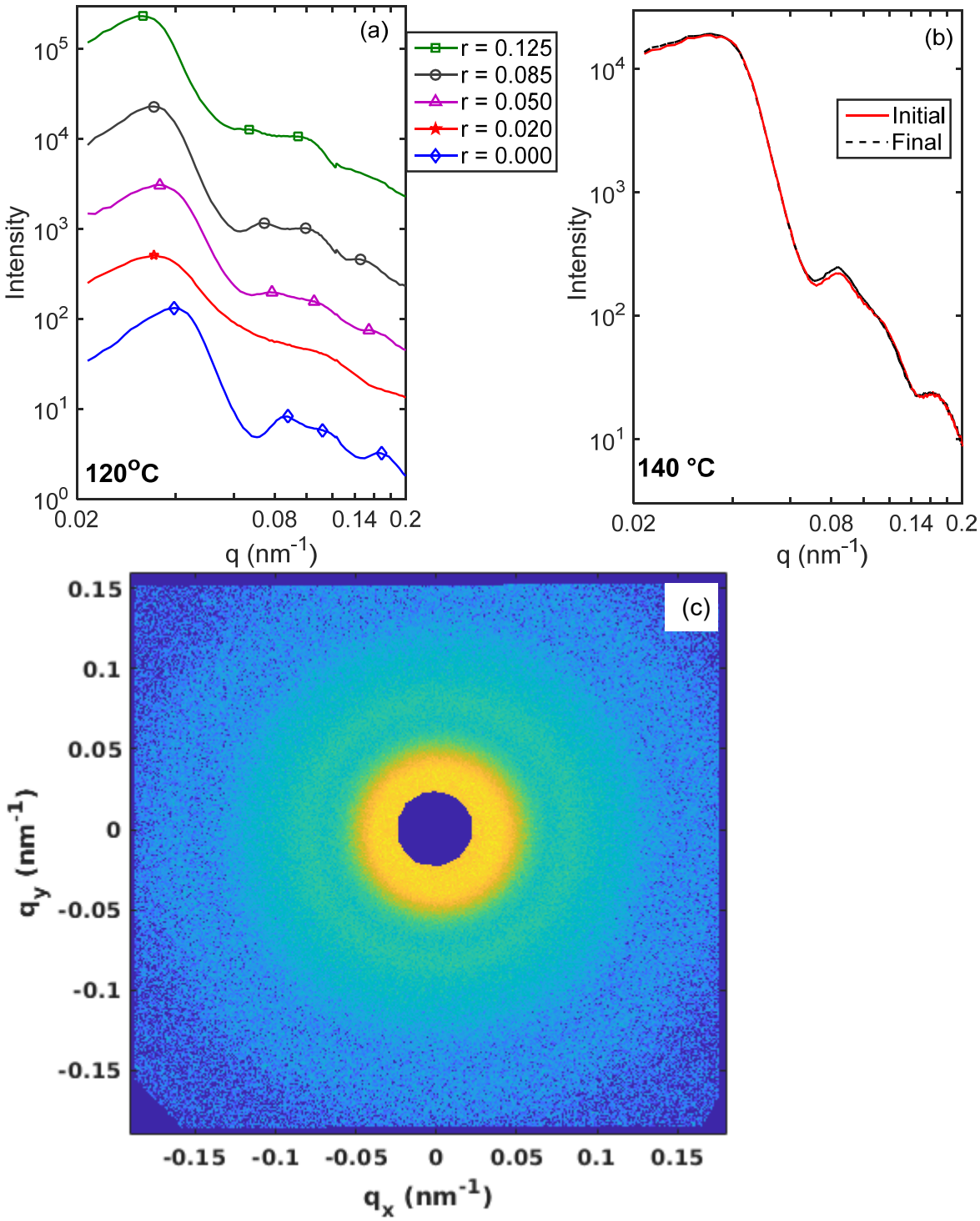

Figure 1. 1D static SAXS intensity profiles obtained (a) at 120 ˚C for different salt concentrations, r (mol_{Li^+}/mol_{EO}), of SEO-LiTFSI, and (b) at 140 °C and r = 0.02 from the beginning and end of data collection. (c) Average two-dimensional scattering pattern corresponding to the experiment in b.

The primary scattering peak (q^*) is a function of salt concentration and temperature. In Figure 2a, the addition of LiTFSI salt to the SEO dramatically shows an increase in the domain spacing ($d = \frac{2\pi}{q^*}$). As shown in Figure 2a, an increase in salt concentration from r = 0 to 0.125 mol_{Li+}/mol_{EO} results in an average domain spacing increase of 20 ± 3%. Excluding r = 0.02 mol_{Li+}/mol_{EO}, d has a linear dependence on r. As described in the experimental section, we have taken careful steps to prevent water contamination in our samples and think that the results at r = 0.02 mol_{Li+}/mol_{EO} are real. This result can be explained by a phase-separation gap at low ion volume fraction that is predicted by computational work from Olvera de la Cruz's group[46] and supported by experimental results from Balsara's group[47]. X-ray scattering was conducted with decreasing temperature steps in order to avoid possible thermal annealing effects that might occur with increasing temperature experiments. Unlike other salt concentrations, only a broad higher order peak is apparent in the r = 0.02 profile at 120 °C shown in Figure 1a, the location of which is not readily discernable. Multiple distinct higher order peaks are apparent in the r = 0.02 profile at 140 °C shown in Figure 1b. This indicates that there is some complexity to BCP microstructure at low salt concentration that would benefit from a more detailed study between r = 0 and r = 0.05.

To better understand the dependence of domain spacing on temperature and salt concentration, it is useful to consider the effect of these parameters on segregation strength, the product of the effective Flory-Huggins Interaction parameter (χ_{eff}) and the degree of polymerization (N). χ_{eff} between PS and PEO is a weak function of temperature.[48] It has also been studied in lower M_N SEO polymers (less than 15 kg/mol) containing LiTFSI. In such polymers, the effective interaction parameter, χ_{eff}, was observed to increase linearly with r over a

limited range of salt concentration[31, 43] but to have a saturated exponential growth dependence over a broader r range, according to the following equation.[47]

$$\chi_{eff} = A/T + B/(T \cdot N) + C \cdot T/N\,(1 - \exp(-D \cdot T \cdot r/N)) \quad (5)$$

For SEO, A = 10.2 K, B = 1.85 x 10^3 K, C = 1.01 x 10^{-2} K^{-1}, and D = 22.4 K^{-1}. In order to calculate N, density of each phase is needed. For the salt-free sample, data from Zoller and Walsh can be used (see the supporting information for details).[35] The density of PEO as a function of salt concentration, ρ(r), was determined in the same work that developed equation 5.[47] It was found to deviate by less than 5% from volume additivity, but in a non-monotonic fashion. N is then the sum of the degree of polymerizations of the blocks, N_{PEO} and N_{PS}, which can be calculated as follows:[47]

$$N_i(T,r) = \frac{M_{N,i}}{\rho_i(T,r) N_A v_{ref}}. \quad (6)$$

where N_A is Avogadro's number, and v_{ref} is a reference volume, taken to be 0.1 nm^3. The properties of our SEO-LiTFSI block copolymer electrolytes at 140 °C are reported in Table 1. In all cases, χN is greater than 100. Based on the phase diagram of symmetric diblock copolymers,[49] χN greater than 60 can be considered strongly phase segregated.

Table 1. Properties of SEO-LiTFSI at 140 °C.

$r = \frac{[Li^+]}{[EO]}$	ρ_{PEO}[a] (g/cm^3)	N_{PEO}[b]	N_{Total}[c]	χ[b]	χN
0.000	0.837	2261	4847	0.0256	124
0.050	1.203	1574	4160	0.0257	109
0.085	1.233	1535	4121	0.0258	106
0.125	1.444	1315	3901	0.0258	101

[a] Taken from Zoller and Walsh[35] for r = 0 and Teran and Balsara[47] for $r \neq 0$.
[b] Calculated according to Teran and Balsara[47]. Accounts for temperature and salt concentration.
[c] $N_{Total} = N_{PEO} + N_{PS}$. N_{PS}(140 °C) = 2586.

In the strong segregation limit (relevant for our 247 kg/mol SEO), block copolymer d is predicted to scale with $\chi^{1/6}$ (and therefore $r^{1/6}$ for a linear dependence of χ on r).[50, 51] However, the work in reference [47] predicts that salt concentration will have negligible effect on χ in the high M_N limit. The linear dependence of d on r observed in Figure 2a bears out this prediction. In other words, the addition of salt for the most part only serves to increase the volume of the PEO phase, but does not impact χ. The linear regressions in Figure 2a have slopes ranging from 222 nm $mol_{EO}/mole_{Li}$ at 180 °C to 306 nm $mol_{EO}/mole_{Li}$ at 120 °C. The intercepts range from 159 nm at 100 °C to 171 nm at 180 °C. The slope and intercept of the 140 °C data are 249 nm $mol_{EO}/mole_{Li}$ and 159 nm, respectively. Complete regression results are reported in Table S1. Linear dependence of d on r would be expected based on volume additivity, but the observed increase in d is about 2/3 of that predicted by volume additivity. For example, a 30% increase in d from $r = 0$ to 0.125 mol_{Li+}/mol_{EO} is predicted. See supporting information for details. The over-prediction of volume additivity suggests either an effect of the anisotropy of the lamellar morphology or a negative volume change upon mixing, which might be expected due to PEO-salt complexation. Quantitative modeling beyond the zeroth order approximation of volume additivity would require more accurate measurement of density than is afforded by domain spacing. Since the primary focus of this work is dynamics, more detailed modeling of domain size is not attempted. In the future, we will explore this further with other morphologies. The use of high M_N polymer electrolyte in this work is motivated by good battery performance[4] due to superior mechanical properties. As shown in Figure 2b, such high M_N results in small grains with only minor, non-monotonic effect of salt on grain size. As described in the supporting information, grain size was calculated using Scherrer analysis[52] (width) of the primary scattering peak (see Figure S7). We also report the temperature dependence of the domain spacing in

Figure S8. There is some scatter in the data, but for the most part the temperature-dependence of the domain spacing agrees with the calculation based on the thermal expansion coefficient of SEO (solid lines). This suggests that in addition to the high thermodynamic penalty for chain mixing that is present in strongly segregated BCPs, the chains are highly entangled such that diffusion along the domain interfaces is not possible on the timescale of the experiments (see Discussion section for more detail). Thus, domain spacing cannot respond to the, albeit weak, temperature dependence of χ, but can only increase due to thermal expansion. The domain spacing reported in Figure S8 qualitatively agrees with reference [47], where volume additivity over-predicts specific volume below r = 0.085 and under-predicts specific volume above r = 0.085.

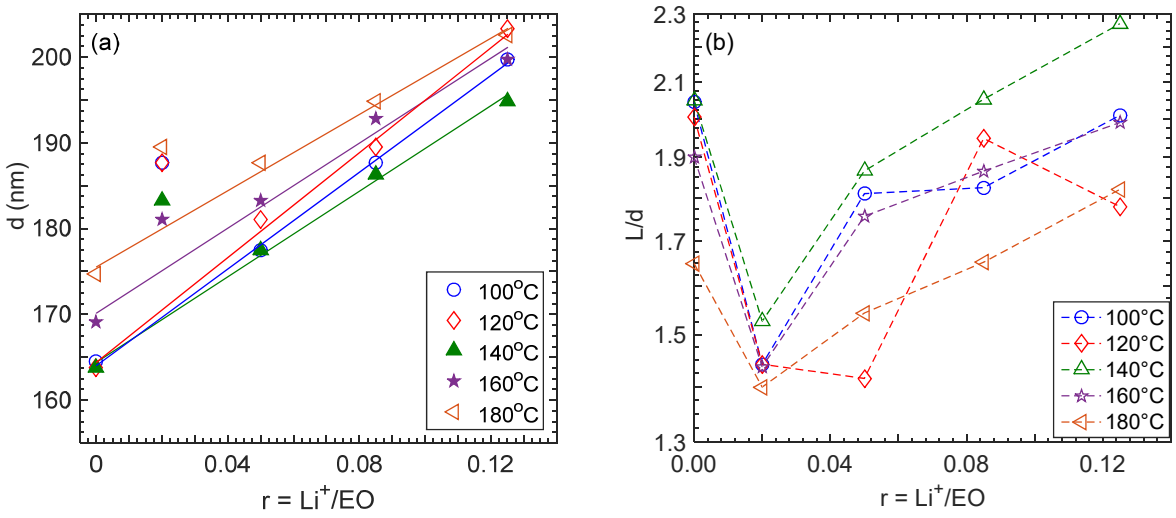

Figure 2. (a) Domain spacing, *d*, of SEO-LiTFSI as a function of salt concentration at different temperatures. Solid lines are linear regressions to each data set with r = 0.02 mol_{Li+}/mol_{EO} excluded. (b) Ratio of grain size to domain spacing, *L/d*, of SEO-LiTFSI as a function of salt concentration at different temperatures. Error bar are smaller than the data symbols.

3.2 Structural Dynamics (XPCS results)

Figure 3 shows the average intensity autocorrelation functions (g_2) versus delay time on a logarithmic scale at different temperatures for three salt concentrations within a narrow q-range around the primary scattering peak ($0.044 nm^{-1}$). These data extended over two decades in delay time, from the shortest delay time of 1 s to a longest delay time of 256 s. The g_2 values at short delay times compare well with the scattering contrast determined by the aerogel standard, indicating the absence of faster relaxation processes that occur below the shortest delay time accessible with the experimental setup employed. Decay of g_2 was only observed on this time scale above the glass transition temperature (T_g) of PS. In fact, measurements at 80 °C and 25 °C shown in Figure S9 were completely flat, without even the partial decay of g_2 seen at 100 °C. At 100 ˚C (very close to the glass transition temperature of the PS block), slow dynamics of the SEO-LiTFSI system was observed for all salt concentrations. This may be due to the fact that this SEO is majority PS.

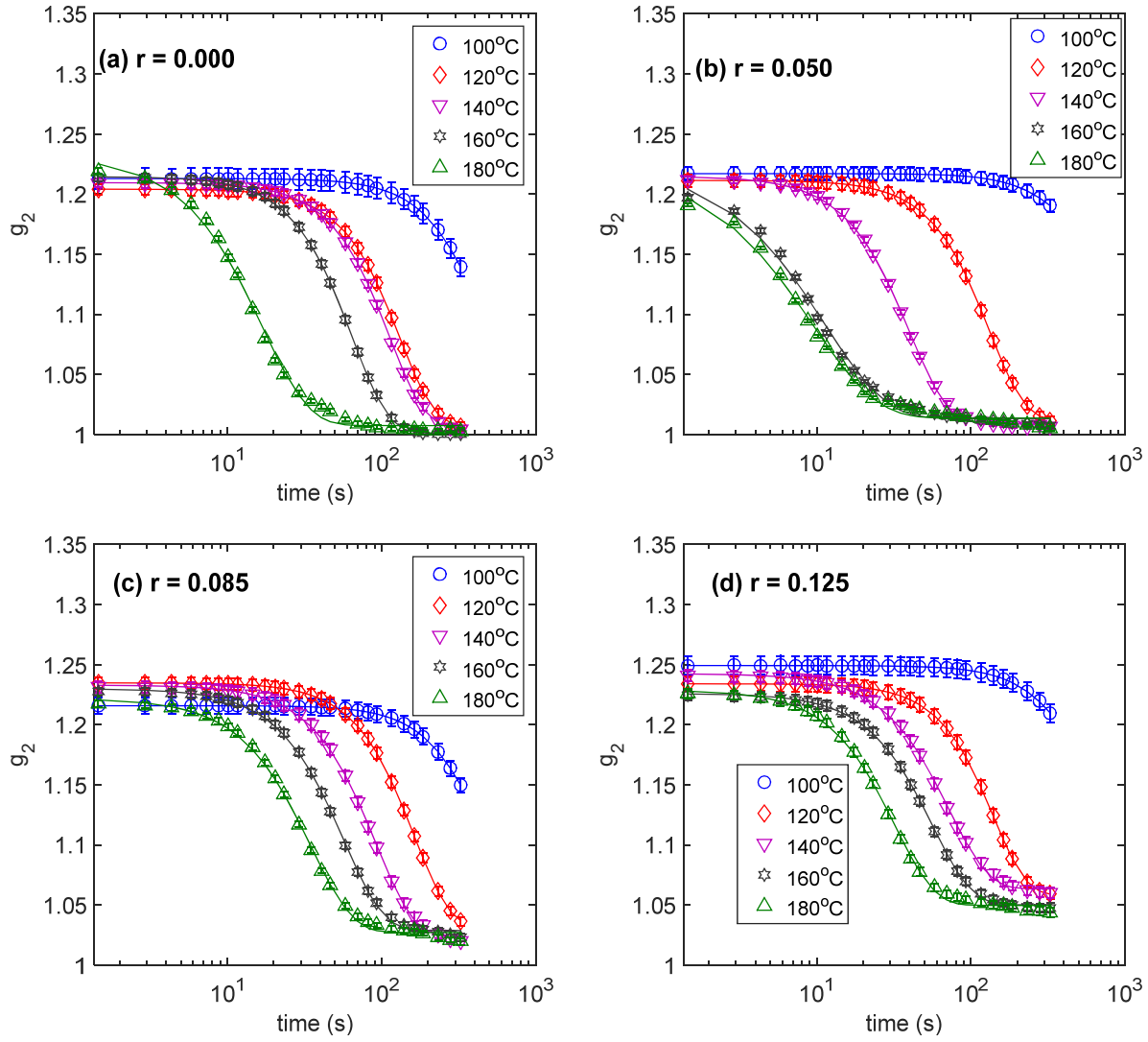

Figure 3. Autocorrelation functions obtained from SEO electrolytes of different salt concentrations: (a) r = 0.000, (b) r = 0.050, (c) r = 0.085, and (d) r = 0.125 mol_{Li+}/mol_{EO}. Solid lines denote the compressed exponential fits. q range is 0.04031 to 0.04670 nm^{-1}.

One of the adjustable parameters in the regressions of equation 4 to data in Figure 3 is the stretching exponent, β. As shown in Figure 4, it is independent of q and r but shows a slight decrease with increasing temperature. The values of β decrease from approximately 2 at 100 °C to about 1.6 at 160 °C. This indicates a compressed, faster-than-exponential form consistent with other observations of hyperdiffusive behavior.[53, 54] β does take on a value close to 1 at the highest temperatures and lowest salt concentrations, which is indicative of a single relaxation process.

To define hyperdiffusive motion it is useful to relate position (of a particle or differential control volume of a material) to time: $\langle x^2 \rangle^{1/2} \propto t^n$. Diffusive behavior occurs when n = ½. Hyperdiffusive behavior describes any motion in which n > 1/2. An example is Case II diffusion of solvent molecules in glassy polymer that is plasticized by the solvent. An additional driving force beyond random thermal motion could also cause hyperdiffusive motion. Examples, could be residual stress gradients within a material or interfacial energy between BCP phases.

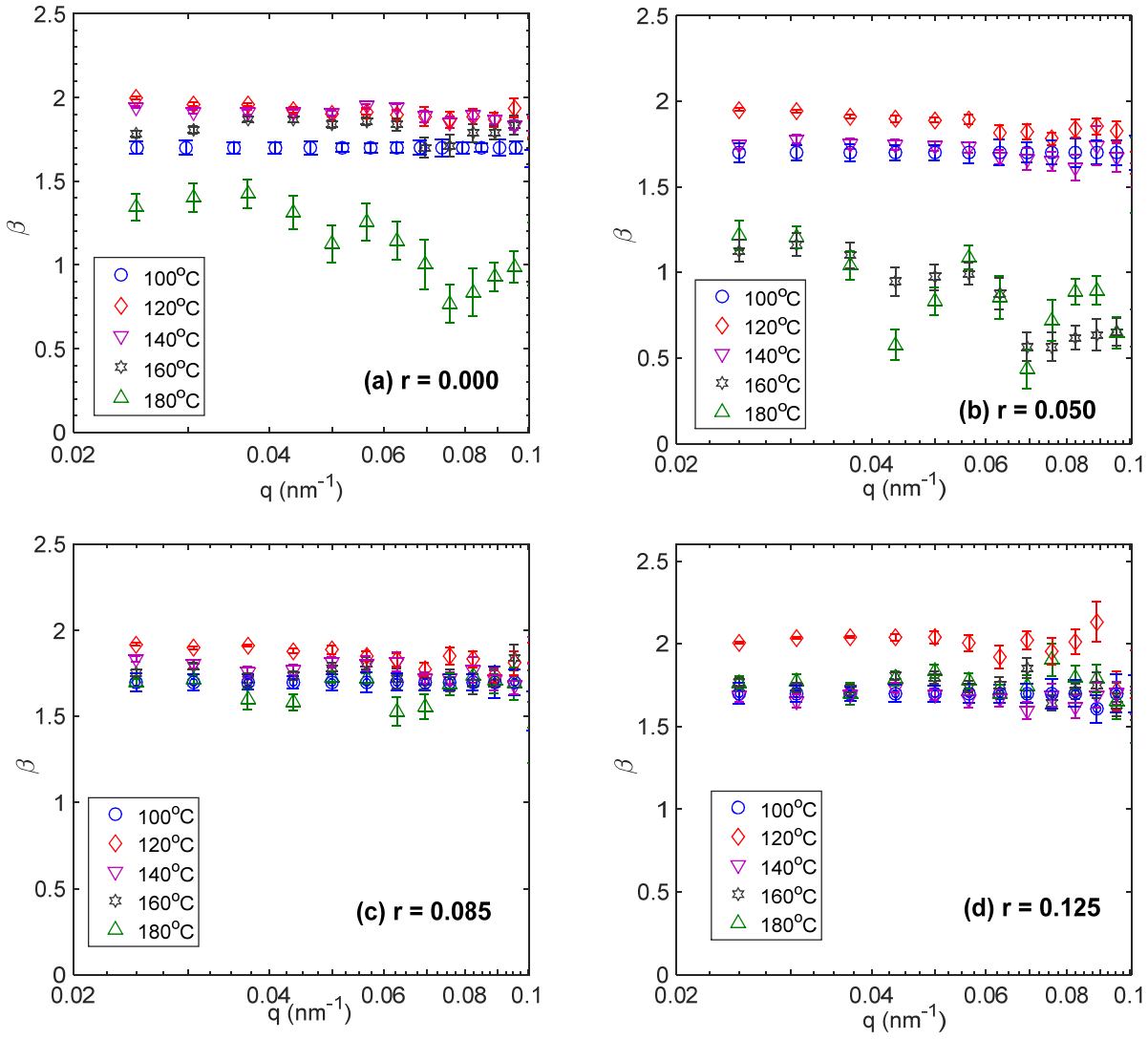

Figure 4. Exponent from KWW fit at different temperatures for SEO-LiTFSI of (a) r = 0.000, (b) r = 0.050, (c) r = 0.085, and (d) r = 0.125 mol_{Li+}/mol_{EO}.

The q-dependence of the structural relaxation times is shown in Figure 5 at four salt concentrations (r = 0.00, 0.05, 0.085, and 0.125) between 100 and 180 ˚C. The structural relaxation time, τ_{st}, decreases monotonically with an increase in temperature for all salt concentrations.

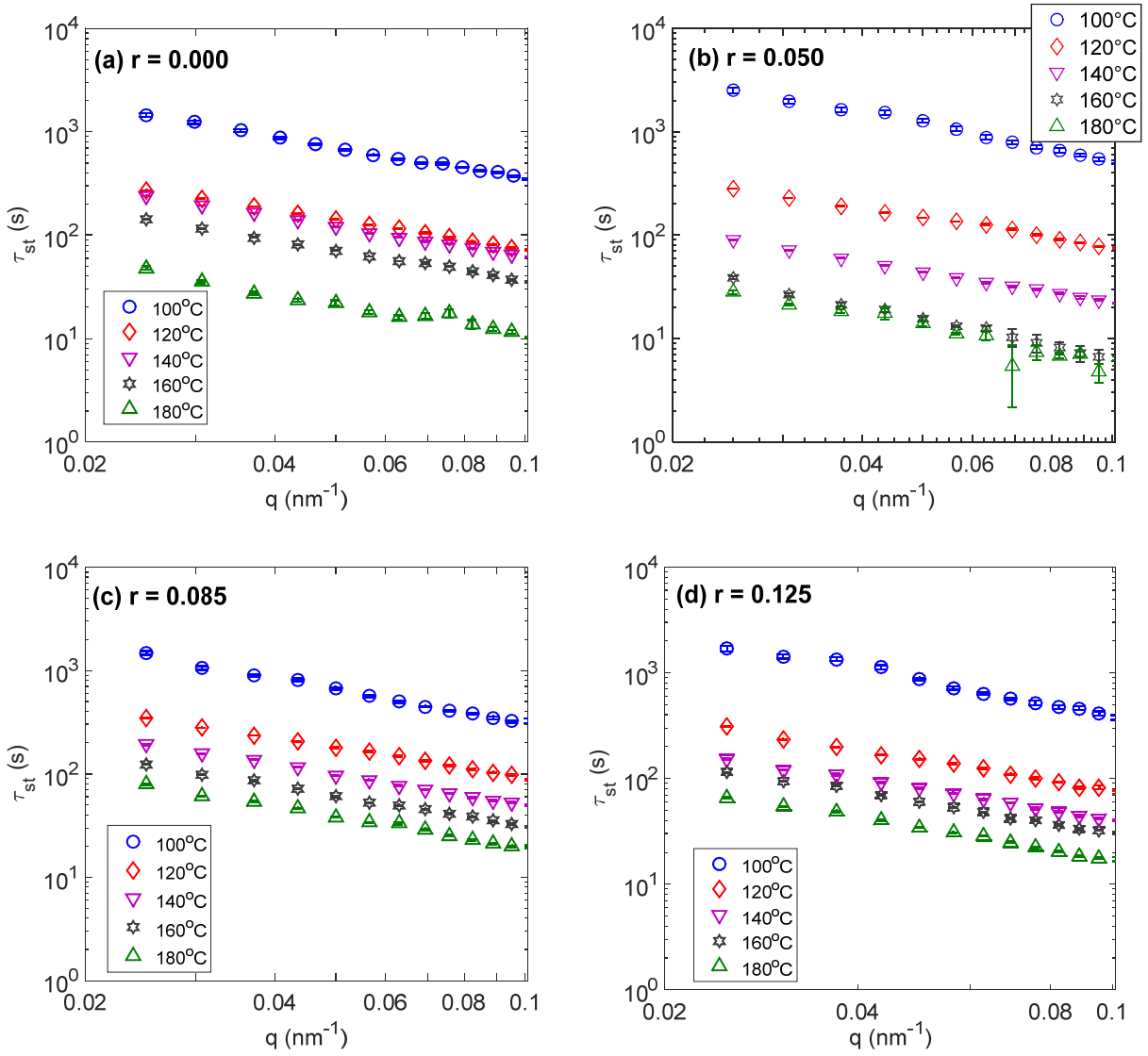

Figure 5. Structural relaxation time, $\tau_{st}(q)$, versus wave vector, q, at different temperatures (a) r = 0.000, (b) r = 0.050, (c) r = 0.085, and (d) r = 0.125 mol_{Li+}/mol_{EO}.

At each salt concentration, the decrease is at least an order of magnitude from 100 ˚C to 180 ˚C. However, $\tau(q)$ scales approximately with q^{-1}, with exact power, γ, reported in Figure 6 in the range of -0.6 < γ < -1.2. Similar behavior has been reported in soft glassy systems, and such hyperdiffusive behavior has been attributed to local strain gradients (see discussion for details).[55-65]

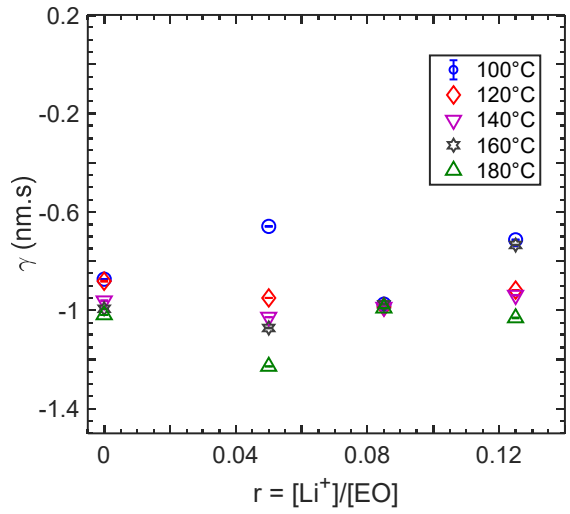

Figure 6. Slope from log-log plot in Figure 5 of structural relaxation time, $\tau(q)$, versus wave vector, q, versus salt concentration, r.

Regarding the presence of salt in the polymer, PEO lithium complexes result from the solvation of the LiTFSI salt by ether oxygens. This complexation state is a strong function of salt concentration,[33, 66, 67] which in turn affects the PEO chain mobility.[8] However, there appears to be only a weak relationship between the structural relaxation and salt concentration (Figure S10). This indicates that salt does not significantly affect BCP electrolyte grain dynamics over the small range of grain sizes examined in this study. An investigation with a larger range of grain sizes is needed to determine if ionic conductivity correlates with grain dynamics at a fixed salt concentration.

3.3 Rheological properties of SEO-LiTFSI

In an attempt to uncover the physical origins of the structural relaxation observed with XPCS and gain insight into the effect of salt on mechanical properties, rheological studies of SEO-LiTFSI were conducted. The frequency-dependent linear viscoelastic properties of SEO-LiTFSI electrolytes at 120°C are reported as a function of *r* in Figure 7. Strain amplitude of 1%, which was confirmed to be well inside the linear viscoelastic regime, was used for all experiments. Singh *et al.*[68] reported no observable change in shear modulus upon addition of a small amount of salt (SEO-LiTFSI). We observed similar behavior at low salt concentration in SEO but do see an effect on rheological properties at higher salt concentrations. The amount of salt in the SEO affects both the storage and loss moduli at all frequencies. With an increase in the salt concentration from r = 0.02 to r = 0.125, the storage modulus decreases by a factor of three as shown in Figure 7(a). Even at r = 0.17, SEO-LiTFSI remains a viscoelastic solid ($G' > G''$). Although the data in Figure 7 span over five decades in frequency, the frequency window is still too small to explore all relevant relaxation phenomena. In particular, segmental relaxations and terminal (chain diffusion) relaxations are not directly accessible with the rheometer.

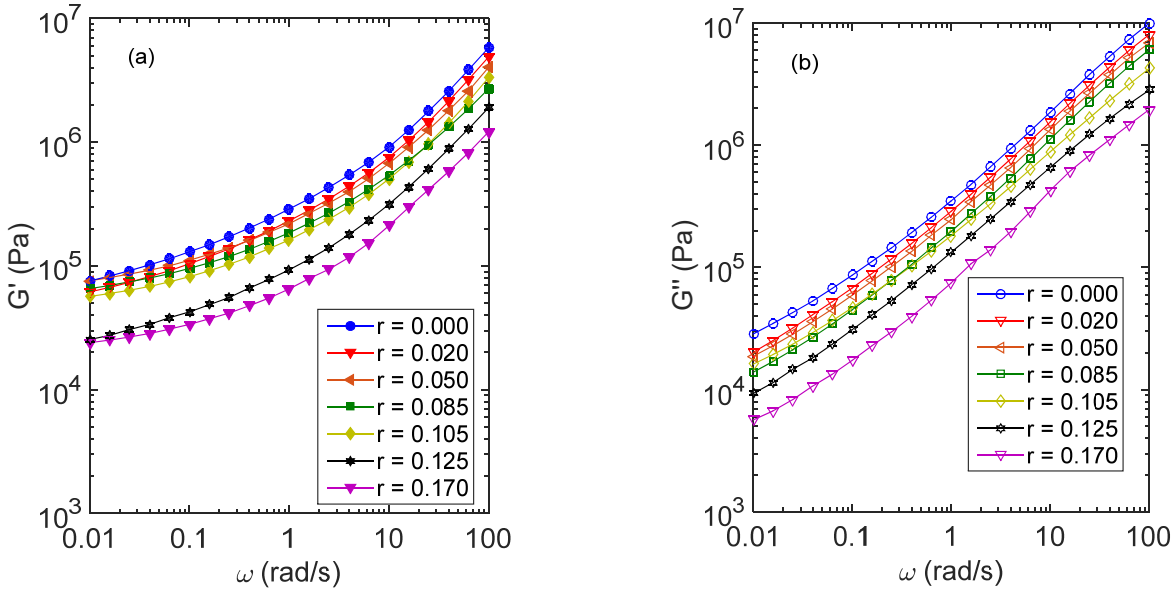

Figure 7. Shear rheology data for SEO-LiTFSI at different salt concentrations for 120 ˚C (a) storage modulus (G') and (b) loss modulus (G'').

At a reference temperature of 120 °C, lower and higher temperature data were horizontally shifted based on WLF time–temperature superposition parameters determined using the closed-form mathematical algorithm (CFS) program by Gergesova et al.[69] According to the time-temperature superposition (TTS) principle for viscoelastic polymers, time and temperature are equivalent to the extent that dynamic data at one temperature can be superimposed on data at another temperature by shifting the curves along the time axis. The horizontal shift factors, $a_T(T)$, were determined by the CFS program using the WLF equation in equation 7.

$$Log(a_T) = \frac{-C_1\left(T - T_{ref}\right)}{\left[C_2 + \left(T - T_{ref}\right)\right]} \tag{7}$$

By shifting the individual spectra measured at different temperatures (shown in Figure S11) to the reference temperature (T_{ref}), a much wider scale of frequency can be accessed. The WLF parameters are reported in Table 2. For simplicity, vertical shifts were not used. Including such

minor correction for temperature dependence of density resulted in less than 2% difference in the master curves, i.e. thermal expansion coefficient of both phases (PEO and PS) is similar. The high molecular weight SEO samples have an inaccessible T_{ODT}, estimated to be above 1000 °C. The lack of a structural transition allows for the use of time-temperature superposition.[70]

Table 2.WLF parameters for time-temperature superposition of SEO and SEO-LiTFSI at a reference temperature of 120 °C.

$r=\frac{[Li^+]}{[EO]}$	C1	C2
0.000	3.24	36.47
0.020	4.63	40.85
0.050	3.21	26.62
0.085	4.77	48.18
0.105	2.95	27.75
0.125	4.25	30.88
0.17	2.92	25.42

The master curves constructed by superpositioning the frequency sweeps measured above $T_{g,PS}$ are shown in Figure 8 and Figure S12 for all salt concentrations investigated. An appropriate way to compare the dynamics of SEO-LiTFSI for different salt concentrations and temperatures is to focus on the rheological regimes described below. The four regimes usually observed in rheology of entangled homopolymers (from high to low frequency) are the glass plateau, a transition regime, the entanglement regime (rubbery plateau), and a terminal regime where viscous flow is observed. Intersections of the master curves of the storage and loss moduli delineate the boundaries between these regimes and correspond to three important relaxation times: relaxation time of one segment of the equivalent freely jointed chain – Kuhn monomer,

τ_{seg}; Rouse relaxation time of chain segments between entanglements, τ_e; and entangled chain diffusion or reptation relaxation time, τ_{rep}. The segmental and entanglement relaxation times are denoted in the master curve of SEO, Figure 8a.

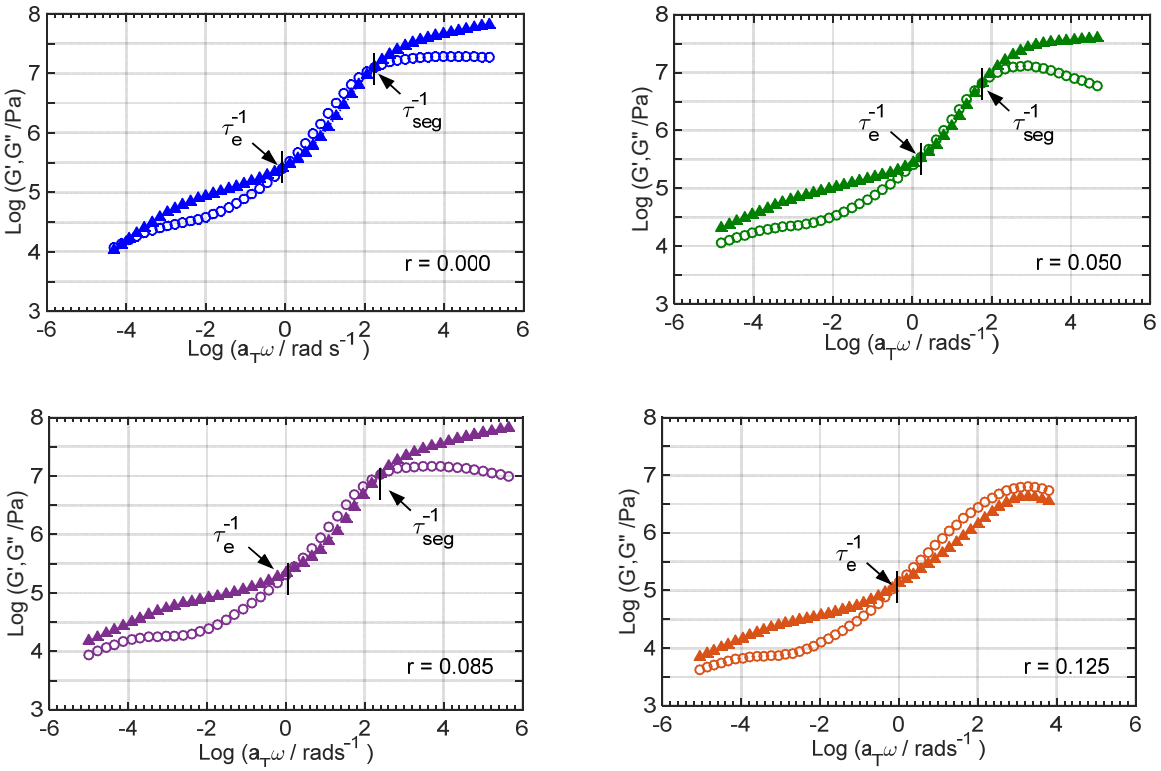

Figure 8. Storage and loss moduli of SEO-LiTFSI at different salt concentrations as a function of time-temperature-shifted frequency, $a_T\omega$, using a reference temperature of 120 °C. Filled symbols are *G*' and open symbols are *G*".

The viscoelastic behavior of SEO was dominated by the PS block at medium and high frequencies. As the majority phase with much higher T_g than PEO, PS dominates the mechanical behavior at medium and high frequency. A comparison of the viscoelastic behavior of PS with pure SEO is shown in Figure 9 with both TTS data sets constructed at a reference temperature (T_{ref}) of 120 °C. The shear moduli of SEO are a small but noticeable amount lower than the PS

due to the presence of the continuous PEO phase. The reptation time and terminal regime are not observed in SEO due to the nanostructure preventing flow in these low-strain oscillatory experiments. Such solid-like behavior in the terminal regime (storage modulus greater than loss modulus) is attributed to the strongly phase-separated morphology.[71, 72]

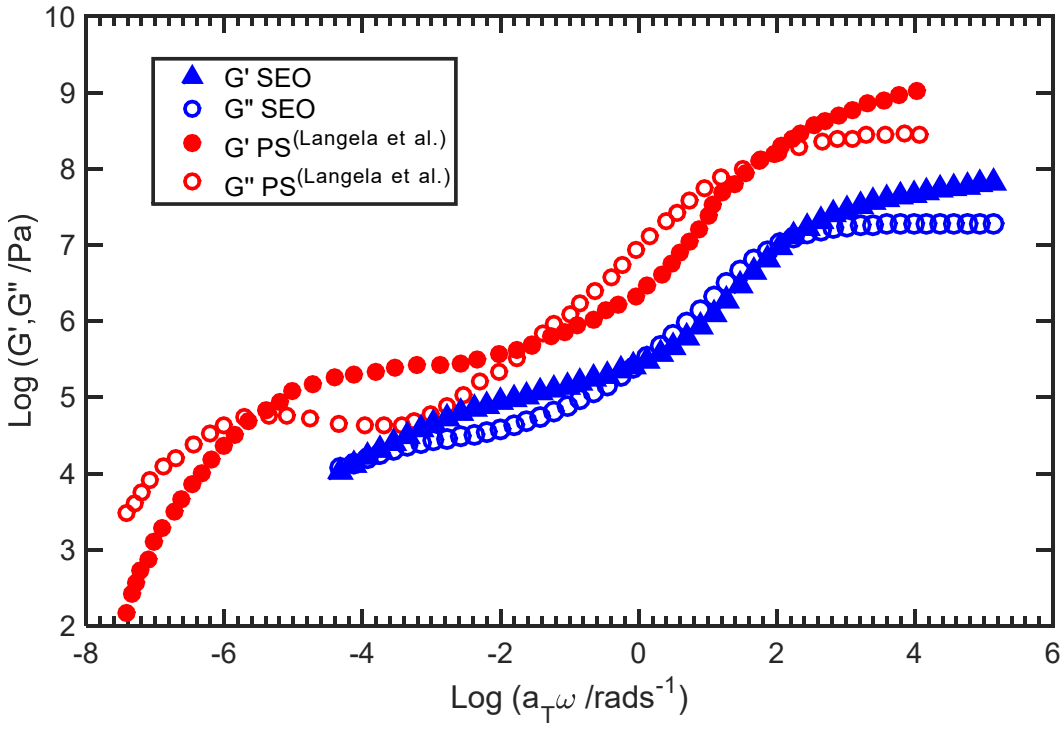

Figure 9. Master curve comparison of SEO and polystyrene (showing PS dominating the storage and loss moduli of SEO).[73]

At high frequencies (above τ_{seg}), the SEO-LiTFSI systems exhibit glassy behavior. G' is greater than the G" indicating a viscoelastic solid-like behavior. Although an actual plateau is not reached, we report the modulus at the highest frequency, G' = 6 x 10^7 Pa. As shown in Figure 9, this is less than the modulus of 4 x 10^8 Pa for PS at a similar frequency increment above τ_{seg} (PS).[73-75] At 120 °C, the segmental relaxation time of SEO (τ_{seg} = 4 x 10^{-2} s) was lower than PS homopolymer (τ_{seg} = 10^{-1} s). This difference is expected due to the contribution from the PEO

block ($\tau_{seg} = 10^{-10}$ s)[76, 77]. A simple, effective medium argument predicts

$$G'_{SEO} = \frac{2}{3}\left(\frac{\phi_{PS}}{G'_{PS}} + \frac{\phi_{PEO}}{G'_{PEO}}\right)^{-1} + \frac{1}{3}\left(\phi_{PS} G'_{PS} + \phi_{PEO} G'_{PEO}\right), \quad (8)$$

where ϕ_{PEO} is the volume fraction of the PEO + LiTFSI phase. Since G'_{PEO} is orders of magnitude less than G'_{PS}, the expression simplifies to $G'_{SEO} = 1/3\phi_{PS}G'_{PS} = 7 \times 10^7$ Pa for neat SEO ($\phi_{PS} = 0.58$), which agrees well with experiment. Based on volume additivity and the fact that LiTFSI selectively swells only the PEO phase, the prediction can be used to explain the effect of salt on SEO-LiTFSI modulus. The decrease of modulus with salt addition is simply caused by ϕ_{PS} decreasing with increasing salt concentration. With increasing salt concentration the prediction quality worsens. This could be due to uncertainty in volume additivity or perhaps the loss of some percolated PS as its volume fraction decreases. We do not have an explanation for the lack of a τ_{seg} intersection at r = 0.105 and 0.125 mol_{Li+}/mol_{EO} but do point out that there is a gradual trend in the shape of the master curves with salt concentration (see Figures 8 and S12).

At medium frequency, between τ_{seg} and τ_e, there is a liquid-like transition region. Immediately below τ_e, the expected entanglement plateau in G' is sloped, with a value of approximately 5 MPa. In constrast to the PS data, the SEO and SEO-LiTFSI samples do not display a τ_{rep} nor terminal flow, but rather both *G*' and *G*" scale as $\omega^{1/2}$. This is attributed to the phase-separated structure and agrees with other reports of unaligned lamellar block copolymers.[78, 79] The soft glassy rheology model predicts that at low frequency *G*' and *G*" both scale as ω^{x-1} when $1< x < 2$. Interactions between different structurally rearranging regions are subsumed into this dimensionless noise temperature, *x*.[58-60] With increasing *r*, the low-frequency slope of log(*G*') versus log(ω) of SEO-LiTFSI samples exponentially decays from the salt free value of 0.47 to an asymptotic value of 0.28 at high salt concentration. Note that *G*' was used

rather than G" due to the linear region (on a log-log plot) spanning over a wider frequency range. These results indicate a decrease of x upon addition of salt. It is reasonable to expect x to be proportional to T/T_{ODT}. Therefore, a decrease of x with addition of salt is likely driven by an increase in T_{ODT}. Structural mobility largely dictates the low frequency mechanical response. Based on XPCS measurements, the effect of grains on the rheological response extends at least up to 10^{-2} Hz. This explains why the entanglement plateau of SEO is sloped rather than being flat like the entanglement plateau of PS in Figure 9.

Another study of BCP rheology used poly(styrene-b-2-vinylpyridine), PS-b-P2VP, with components that have similar thermo-rheological behavior. The grain contribution (extrapolated from low frequency) and PS contribution were subtracted from the BCP master curve to yield the P2PV chain contribution.[79] Due to the significantly differents T_g's of our components, we have not attempted this. The entanglement relaxation time for PEO at 75 ˚C has been reported as 1.5 x 10^{-8} s (M_N = 932 kg/mol)[76] and that of PS at 110 °C has been reported as 102 s (M_N = 96 kg/mol).[75] As shown in Figure 10a, the SEO entanglement relaxation time is essentially the same as homopolymer PS and is not affected by the presence of salt. Due to the much faster dynamics of PEO, it only makes significant contribution to rheological response at the highest frequencies accessed with time-Temperature superposition. A more appropriate method for measuring PEO dynamics is neutron spin echo spectroscopy. We have on-going work making such measurements, which are important for designing better polymer electrolytes. The dynamics of the PS phase is important for conferring high mechanical strength to resist lithium dendrite growth, whereas the dynamics of PEO is important for facile ion transport.

4. Discussion

A quantitative comparison of the temperature dependence of the entanglement, τ_e, and structural relaxation, τ_{st}, times is shown in Figure 10b. While entanglement relaxation times show a good fit with the Vogel-Fulcher-Tammann (VFT) equation (equation 9),[80] structural relaxation times show an Arrhenius behavior (equation 10) at all salt concentrations.

$$\tau_e = \tau_{e,o} \exp\left\{\frac{b}{T - T_o}\right\} \tag{9}$$

$$\tau_{st} = \tau_{st,o} \exp\left\{\frac{E_a}{RT}\right\} \tag{10}$$

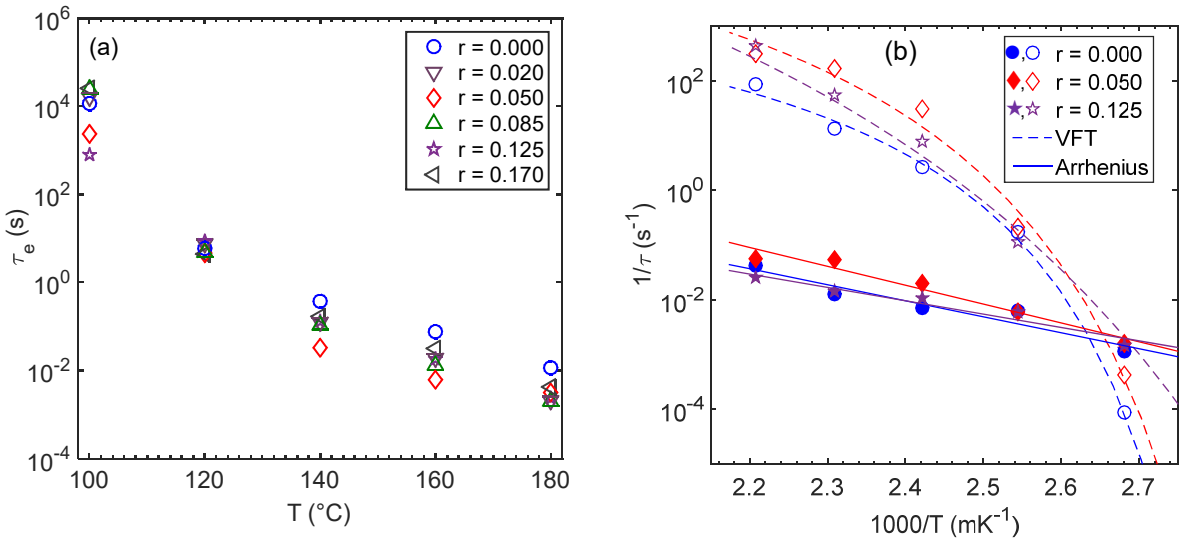

Figure 10. (a) Entanglement relaxation time from rheology. (b) Arrhenius plot of SEO-LiTFSI relaxation rates for different salt concentrations. Open symbols are entanglement relaxation rates from rheology, $1/\tau_e$, and filled symbols are structural relaxation rates from XPCS, $1/\tau_{st}$. Dashed curves are VFT fits to $1/\tau_e$, and solid lines are Arrhenius fits to $1/\tau_{st}$. Error bars of one standard deviation are smaller than the data symbols and therefore not shown.

In equation 9, T_o is the so-called Vogel temperature, b is the energetic term, and $\tau_{e,o}$ provides the high-temperature limit of the relaxation time. In equation 10, $\tau_{st,o}$ is the high-temperature limit of the relaxation time, E_a is the activation energy, and R is the gas constant (8.314 J mol^{-1} K^{-1}). The dashed lines in Figure 10(b) correspond to VFT fits. The resulting VFT parameters for the regressions to the entanglement relaxation time data of SEO-LiTFSI are shown in Table S2. The Arrhenius parameters from regressions to structural relaxation time data from XPCS are presented in Table S3. Like the relaxation times from the two experiments, both sets of parameters in Tables S2 and S3 have no clear trend with salt concentration. To empirically deconvolute structural and entanglement contributions to the rheological results, we examined the ratio Rb/E_a. It increases quadratically with r (Figure S13). This analysis excludes r = 0.02 mol_{Li+}/mol_{EO}, where it is not clear that the block copolymer electrolyte is ordered. So, although salt decreases modulus by increasing PEO volume fraction, it also appears to increase the activation energy for chain dynamics. In other words, the modulus decreases due to change of structure, whereas the activation energy for entanglement dynamics increases due to the ionic crosslinking of the ether units in the PEO backbone (PEO-ion complexation). The latter result aligns with other literature reports, such as the increase of PEO T_g with increasing salt content.[81-83] The activation energy from XPCS was about one order of magnitude higher than that from rheology for all the salt concentrations studied.

Several pieces of evidence support the assertion that cooperative dynamics is being measured by XPCS. Cooperative dynamics means a large ensemble of segments moving in unison, grain rotation is an example that is depicted schematically in Figure S14. First, the structural relaxation measured by XPCS is significantly slower than the entanglement relaxation measured by rheology at temperatures above T_g. This ratio diverges to large values at high temperatures, due

to the weak thermal activation energy of τ_{st} and the strong temperature dependence of τ_e (Figure 10b). Second, the compressed exponential and the linear dependence of τ_{st} on q indicates that it is not diffusive dynamics that is being measured. We also know that chain diffusion is not responsible for this relaxation because the relaxation time from XPCS (approximately 200 s at 120 °C) is 10 times faster than arm retraction of the PS block (and many orders of magnitude faster than PEO arm retraction). Arm retraction determines chain diffusion along the interface in strongly segregated block copolymers.[84] XPCS appears to be measuring pressure-driven defect velocity rather than chain diffusion. This can be in the form of grain growth, grain rotation, low-angle grain boundary unzipping,[85] and surface fluctuations.[18, 86] Grain rotation is the most likely physical explanation for the structural motion observed in our strongly segregated BCPs with XPCS. In the vicinity of scattering maxima, each speckle is associated with a group of aligned lamellae, i.e. a grain, with a particular orientation. If the grain rotates the scattering direction will change. This will cause the speckle to move, or even disappear if the grain rotates into an orientation in which it cannot scatter the coherent incident x-rays. Figure S14 shows a schematic depicting this process.

Another study of defect dynamics with time-resolved AFM found the temperature dependence for such processes was Arrhenius rather than exhibiting VFT-type behavior expected for polymer dynamics near T_g.[87] This agrees with our results shown in Figure 10b, where the temperature dependence of the entanglement relaxation rate (determined by time-temperature shifted rheology) displayed the expected VFT behavior, whereas the temperature dependence of the structural relaxation (determined from XPCS) showed Arrhenius behavior. Finally, we note that the characteristic times from the two techniques are approximately equal at T_g. This might indicate that the length scale of cooperative segment motion in PS is similar to the structural

length scale at T_g, but that collective structural dynamics is on a much different length scale than entanglements at higher temperatures. Experiments with the complementary techniques of XPCS and rheology on a larger range of grain sizes will enable the evaluation of the frequency range over which mechanical properties are impacted by grain disorder.

Interestingly, the structural relaxation has a weak dependence on salt concentration and also lacks the de Gennes narrowing,[88] with a minimum relaxation time nearly corresponding to the optimal salt concentration for ion conduction (Figure S10a). This suggests that there is in fact a connection between BCP grain dynamics and ion conduction. In future work, we will test the hypothesis that cooperative BCP structural dynamics is due to grain rotation by examining structural relaxation as a function of grain size and morphology type.

Conclusions

We have measured the structural and stress relaxation times of diblock copolymer electrolytes for different lithium salt concentrations and temperatures using XPCS and rheology techniques, respectively. The polymer dynamics obtained provide a starting point for investigating other structural conditions within solid-state polymer electrolytes. We observed both structural motion of the system from XPCS measurements and segmental relaxation of the polymer chains from rheology. With increase in the salt concentration, the shear modulus decreased due to change of structure, whereas the activation energy measured from the entanglement dynamics increased due to the ionic crosslinking of the ether units in the PEO backbone. The hyperdiffusive, Arrhenius structural motion observed with XPCS is indicative of a cooperative, glassy dynamics, possibly due to grain rotation. In contrast, the VFT entanglement

motion observed with rheology is indicative of a fundamental polymer chain relaxation. The coincidence of the two relaxation times at $T_{g,PS}$ suggests a fundamental connection between chain and structural motion even in strongly segregated block copolymers. Surprisingly, the rheological response displayed more sensitivity to salt concentration than did the structural autocorrelation, which means that the physical explanation for the connection between grain size and ionic conductivity remains an open question.

Acknowledgments

We are indebted to Prof. N. Balsara and Prof. A. Sokolov for detailed discussions of the XPCS results. This research used resources of the Advanced Photon Source, a U.S. Department of Energy (DOE) Office of Science User Facility operated for the DOE Office of Science by Argonne National Laboratory under Contract No. DE-AC02-06CH11357. S.R. would like to thank NSF CREST award number 1735968 for partial support of this work. D.H. acknowledges NSF DMR award number 1751450 for partial support of this work.

Supporting Information

Tables of regression results and material properties; Figures of NMR and GPC demonstrating lack of beam damage, parametric examination of exponential decay stretching, speckle correlation and 2D scattering patterns, grain size, temperature dependence of domain size, lack of XPCS decay below $T_{g,PS}$, salt dependence of relaxation times, time-Temperature superposition, master curves of additional salt concentrations, salt concentration dependence of activation energy ratio of rheology and XPCS results; Schematic of grain rotation.

References

1. Xu, K. Nonaqueous liquid electrolytes for lithium-based rechargeable batteries. *Chem. Rev.* **2004,** 104, (10), 4303-4417.
2. Berdichevsky, G.; Kelty, K.; Straubel, J.; Toomre, E. The tesla roadster battery system. *Tesla Motors* **2006,** 1, (5).
3. Hallinan, D. T.; Balsara, N. P. Polymer Electrolytes. *Annual Review of Materials Research* **2013,** 43, (1), 503-525.
4. Hallinan, D. T.; Mullin, S. A.; Stone, G. M.; Balsara, N. P. Lithium Metal Stability in Batteries with Block Copolymer Electrolytes. *J. Electrochem. Soc.* **2013,** 160, (3), A464-A470.
5. Hassoun, J.; Scrosati, B. Moving to a Solid‐State Configuration: A Valid Approach to Making Lithium‐Sulfur Batteries Viable for Practical Applications. *Adv. Mater.* **2010,** 22, (45), 5198-5201.
6. Wang, Y.; Sokolov, A. P. Design of superionic polymer electrolytes. *Current Opinion in Chemical Engineering* **2015,** 7, 113-119.
7. Stolwijk, N. A.; Heddier, C.; Reschke, M.; Wiencierz, M.; Bokeloh, J.; Wilde, G. Salt-Concentration Dependence of the Glass Transition Temperature in PEO-NaI and PEO-LiTFSI Polymer Electrolytes. *Macromolecules* **2013,** 46, (21), 8580-8588.
8. Maranas, J. K., Solid Polymer Electrolytes. In *Dynamics of Soft Matter*, Sakai, V. G.; Alba-Simionesco, C.; Chen, S.-H., Eds. Springer: New York, 2012; pp 123-143.
9. Mao, G.; Saboungi, M.-L.; Price, D. L.; Armand, M.; Mezei, F.; Pouget, S. α-Relaxation in PEO− LiTFSI Polymer Electrolytes. *Macromolecules* **2002,** 35, (2), 415-419.
10. Williams, M. L.; Landel, R. F.; Ferry, J. D. The temperature dependence of relaxation mechanisms in amorphous polymers and other glass-forming liquids. *J. Am. Chem. Soc.* **1955,** 77, (14), 3701-3707.
11. Bamford, D.; Reiche, A.; Dlubek, G.; Alloin, F.; Sanchez, J. Y.; Alam, M. A. Ionic conductivity, glass transition, and local free volume in poly(ethylene oxide) electrolytes: Single and mixed ion conductors. *J. Chem. Phys.* **2003,** 118, (20), 9420-9432.
12. Adam, G.; Gibbs, J. H. On Temperature Dependence of Cooperative Relaxation Properties in Glass-Forming Liquids. *J. Chem. Phys.* **1965,** 43, (1), 139-&.
13. Kim, J. H.; Min, B. R.; Won, J.; Kang, Y. S. Analysis of the glass transition behavior of polymer-salt complexes: An extended configurational entropy model. *J. Phys. Chem. B* **2003,** 107, (24), 5901-5905.
14. Chintapalli, M.; Chen, X. C.; Thelen, J. L.; Teran, A. A.; Wang, X.; Garetz, B. A.; Balsara, N. P. Effect of Grain Size on the Ionic Conductivity of a Block Copolymer Electrolyte. *Macromolecules* **2014,** 47, (15), 5424-5431.
15. Villaluenga, I.; Chen, X. C.; Devaux, D.; Hallinan, D. T.; Balsara, N. P. Nanoparticle-Driven Assembly of Highly Conducting Hybrid Block Copolymer Electrolytes. *Macromolecules* **2015,** 48, (2), 358-364.
16. Ryu, H. J.; Sun, J.; Avgeropoulos, A.; Bockstaller, M. R. Retardation of Grain Growth and Grain Boundary Pinning in Athermal Block Copolymer Blend Systems. *Macromolecules* **2014,** 47, (4), 1419-1427.
17. Balsara, N. P.; Dai, H. J.; Watanabe, H.; Sato, T.; Osaki, K. Influence of defect density on the rheology of ordered block copolymers. *Macromolecules* **1996,** 29, (10), 3507-3510.
18. Sikharulidze, I.; Dolbnya, I. P.; Fera, A.; Madsen, A.; Ostrovskii, B. I.; de Jeu, W. H. Smectic membranes in motion: Approaching the fast limits of X-ray photon correlation spectroscopy. *Phys. Rev. Lett.* **2002,** 88, (11).

19. Sutton, M.; Mochrie, S. G. J.; Greytak, T.; Nagler, S. E.; Berman, L. E.; Held, G. A.; Stephenson, G. B. Observation of Speckle by Diffraction with Coherent X-rays. *Nature* **1991,** 352, (6336), 608-610.
20. Pine, D. J.; Weitz, D. A.; Zhu, J. X.; Herbolzheimer, E. Diffusing-Wave Spectroscopy: Dynamic Light-Scattering in the Multiple Scattering Limit. *Journal de Physique* **1990,** 51, (18), 2101-2127.
21. Thurn-Albrecht, T.; Steffen, W.; Patkowski, A.; Meier, G.; Fischer, E. W.; Grübel, G.; Abernathy, D. L. Photon Correlation Spectroscopy of Colloidal Palladium Using a Coherent X-Ray Beam. *Phys. Rev. Lett.* **1996,** 77, (27), 5437-5440.
22. Malik, A.; Sandy, A. R.; Lurio, L. B.; Stephenson, G. B.; Mochrie, S. G. J.; McNulty, I.; Sutton, M. Coherent X-ray study of fluctuations during domain coarsening. *Phys. Rev. Lett.* **1998,** 81, (26), 5832-5835.
23. *Dynamic Light Scattering Application of Photon Correlation Spectroscopy*. Plenum Press: New York and London, 1985; p 420.
24. Ruegg, M. L.; Patel, A. J.; Narayanan, S.; Sandy, A. R.; Mochrie, S. G. J.; Watanabe, H.; Balsara, N. P. Condensed Exponential Correlation Functions in Multicomponent Polymer Blends Measured by X-ray Photon Correlation Spectroscopy. *Macromolecules* **2006,** 39, (25), 8822-8831.
25. Patel, A. J.; Narayanan, S.; Sandy, A.; Mochrie, S. G. J.; Garetz, B. A.; Watanabe, H.; Balsara, N. P. Relationship between structural and stress relaxation in a block-copolymer melt. *Phys. Rev. Lett.* **2006,** 96, (25).
26. Sanz, A.; Ezquerra, T. A.; Hernandez, R.; Sprung, M.; Nogales, A. Relaxation processes in a lower disorder order transition diblock copolymer. *J. Chem. Phys.* **2015,** 142, (6).
27. Jang, W.-S.; Koo, P.; Sykorsky, M.; Narayanan, S.; Sandy, A.; Mochrie, S. G. J. The Static and Dynamic Structure Factor of a Diblock Copolymer Melt via Small-Angle X-ray Scattering and X-ray Photon Correlation Spectroscopy. *Macromolecules* **2013,** 46, (21), 8628-8637.
28. Rizos, A. K.; Fytas, G.; Roovers, J. E. L. Segmental Motion in Poly(styrene-b-1,4-isoprene) Block Copolymers in the Disordered State. *J. Chem. Phys.* **1992,** 97, (9), 6925-6932.
29. Patel, A. J.; Mochrie, S.; Narayanan, S.; Sandy, A.; Watanabe, H.; Balsara, N. P. Dynamic Signatures of Microphase Separation in a Block Copolymer Melt Determined by X-ray Photon Correlation Spectroscopy and Rheology. *Macromolecules* **2010,** 43, (3), 1515-1523.
30. Semenov, A. N.; Anastasiadis, S. H.; Boudenne, N.; Fytas, G.; Xenidou, M.; Hadjichristidis, N. Dynamic Structure Factor of Diblock Copolymers in the Ordering Regime. *Macromolecules* **1997,** 30, (20), 6280-6294.
31. Young, W.-S.; Epps, T. H., III Salt Doping in PEO-Containing Block Copolymers: Counterion and Concentration Effects. *Macromolecules* **2009,** 42, (7), 2672-2678.
32. Thelen, J. L.; Teran, A. A.; Wang, X.; Garetz, B. A.; Nakamura, I.; Wang, Z.-G.; Balsara, N. P. Phase behavior of a block copolymer/salt mixture through the order-to-disorder transition. *Macromolecules* **2014,** 47, (8), 2666-2673.
33. Chintapalli, M.; Le, T. N. P.; Venkatesan, N. R.; Mackay, N. G.; Rojas, A. A.; Thelen, J. L.; Chen, X. C.; Devaux, D.; Balsara, N. P. Structure and Ionic Conductivity of Polystyrene-block-poly(ethylene oxide) Electrolytes in the High Salt Concentration Limit. *Macromolecules* **2016,** 49, (5), 1770-1780.
34. Hadjichristidis, N.; Iatrou, H.; Pispas, S.; Pitsikalis, M. Anionic polymerization: High vacuum techniques. *J. Polym. Sci., Part A: Polym. Chem.* **2000,** 38, (18), 3211-3234.

35. Zoller, P.; Walsh, D. J., *Standard pressure-volume-temperature data for polymers*. Technomic Pub. Co.: Lancaster, PA, 1995; p 412.
36. Oparaji, O.; Zuo, X.; Hallinan Jr, D. T. Crystallite dissolution in PEO-based polymers induced by water sorption. *Polymer* **2016,** 100, 206-218.
37. Sinha, S. K.; Jiang, Z.; Lurio, L. B. X‐ray Photon Correlation Spectroscopy Studies of Surfaces and Thin Films. *Advanced Materials* **2014,** 26, (46), 7764-7785.
38. Papagiannopoulos, A.; Waigh, T. A.; Fluerasu, A.; Fernyhough, C.; Madsen, A. Microrheology of polymeric solutions using x-ray photon correlation spectroscopy. *Journal of Physics-Condensed Matter* **2005,** 17, (25), L279-L285.
39. Giebel, L.; Meier, G.; Fytas, G.; Fischer, E. W. Dynamic Light Scattering from Bulk Poly(n-hexylmethacrylate) Near and Above the Glass Transition. *Journal of Polymer Science Part B-Polymer Physics* **1992,** 30, (11), 1291-1297.
40. Kim, W. G.; Chang, M. Y.; Garetz, B. A.; Newstein, M. C.; Balsara, N. P.; Lee, J. H.; Hahn, H.; Patel, S. S. Effect of quench depth on grain structure in quiescently ordered block copolymers. *J. Chem. Phys.* **2001,** 114, (22), 10196-10211.
41. Oparaji, O.; Minelli, M.; Zhu, C.; Schaible, E.; Hexemer, A.; Hallinan Jr, D. T. Effect of block copolymer morphology on crystallization and water transport. *Polymer* **2017,** 120, 209-216.
42. Sarapas, J. M.; Saijo, K.; Zhao, Y.; Takenaka, M.; Tew, G. N. Phase behavior and Li+ Ion conductivity of styrene-ethylene oxide multiblock copolymer electrolytes. *Polym. Adv. Technol.* **2016,** 27, (7), 946-954.
43. Wanakule, N. S.; Virgili, J. M.; Teran, A. A.; Wang, Z.-G.; Balsara, N. P. Thermodynamic Properties of Block Copolymer Electrolytes Containing Imidazolium and Lithium Salts. *Macromolecules* **2010,** 43, (19), 8282-8289.
44. Hanley, K. J.; Lodge, T. P.; Huang, C. I. Phase behavior of a block copolymer in solvents of varying selectivity. *Macromolecules* **2000,** 33, (16), 5918-5931.
45. Park, M. J.; Char, K.; Lodge, T. P.; Kim, J. K. Transient solidlike behavior near the cylinder/disorder transition in block copolymer solutions. *J. Phys. Chem. B* **2006,** 110, (31), 15295-15301.
46. Sing, C. E.; Zwanikken, J. W.; de la Cruz, M. O. Theory of melt polyelectrolyte blends and block copolymers: Phase behavior, surface tension, and microphase periodicity. *J. Chem. Phys.* **2015,** 142, (3).
47. Teran, A. A.; Balsara, N. P. Thermodynamics of Block Copolymers with and without Salt. *The Journal of Physical Chemistry B* **2014,** 118, (1), 4-17.
48. Eitouni, H. B.; Balsara, N. P., Thermodynamics of Polymer Blends. In *Physical Properties of Polymers Handbook*, Second ed.; Mark, J. E., Ed. Springer: New York, 2007.
49. Matsen, M. W.; Bates, F. S. Unifying weak- and strong-segregation block copolymer theories. *Macromolecules* **1996,** 29, (4), 1091-1098.
50. Almdal, K.; Rosedale, J. H.; Bates, F. S.; Wignall, G. D.; Fredrickson, G. H. Gaussian- to Stretched-Coil Transition in Block Copolymer Melts. *Phys. Rev. Lett.* **1990,** 65, (9), 1112-1115.
51. Helfand, E. Block Copolymer Theory. III. Statistical Mechanics of the Microdomain Structure. *Macromolecules* **1975,** 8, (4), 552-556.
52. Sanoja, G. E.; Popere, B. C.; Beckingham, B. S.; Evans, C. M.; Lynd, N. A.; Segalman, R. A. Structure-Conductivity Relationships of Block Copolymer Membranes Based on Hydrated Protic Polymerized Ionic Liquids: Effect of Domain Spacing. *Macromolecules* **2016,** 49, (6), 2216-2223.

53. Guo, H.; Bourret, G.; Corbierre, M. K.; Rucareanu, S.; Lennox, R. B.; Laaziri, K.; Piche, L.; Sutton, M.; Harden, J. L.; Leheny, R. L. Nanoparticle Motion within Glassy Polymer Melts. *Phys. Rev. Lett.* **2009,** 102, (7).
54. Jang, W.-S.; Koo, P.; Bryson, K.; Narayanan, S.; Sandy, A.; Russell, T. P.; Mochrie, S. G. Dynamics of Cadmium Sulfide Nanoparticles within Polystyrene Melts. *Macromolecules* **2014,** 47, (18), 6483-6490.
55. Cipelletti, L.; Manley, S.; Ball, R. C.; Weitz, D. A. Universal Aging Features in the Restructuring of Fractal Colloidal Gels. *Phys. Rev. Lett.* **2000,** 84, (10), 2275-2278.
56. Chung, B.; Ramakrishnan, S.; Bandyopadhyay, R.; Liang, D.; Zukoski, C. F.; Harden, J. L.; Leheny, R. L. Microscopic dynamics of recovery in sheared depletion gels. *Phys. Rev. Lett.* **2006,** 96, (22).
57. Bellour, M.; Knaebel, A.; Harden, J. L.; Lequeux, F.; Munch, J. P. Aging processes and scale dependence in soft glassy colloidal suspensions. *Physical Review E* **2003,** 67, (3), 031405.
58. Fielding, S. M.; Sollich, P.; Cates, M. E. Aging and rheology in soft materials. *J. Rheol.* **2000,** 44, (2), 323-369.
59. Sollich, P. Rheological constitutive equation for a model of soft glassy materials. *Physical Review E* **1998,** 58, (1), 738-759.
60. Sollich, P.; Lequeux, F.; Hébraud, P.; Cates, M. E. Rheology of Soft Glassy Materials. *Phys. Rev. Lett.* **1997,** 78, (10), 2020-2023.
61. Akcora, P.; Kumar, S. K.; Moll, J.; Lewis, S.; Schadler, L. S.; Li, Y.; Benicewicz, B. C.; Sandy, A.; Narayanan, S.; Ilavsky, J.; Thiyagarajan, P.; Colby, R. H.; Douglas, J. F. "Gel-like" Mechanical Reinforcement in Polymer Nanocomposite Melts. *Macromolecules* **2010,** 43, (2), 1003-1010.
62. Madsen, A.; Leheny, R. L.; Guo, H.; Sprung, M.; Czakkel, O. Beyond simple exponential correlation functions and equilibrium dynamics in x-ray photon correlation spectroscopy. *New Journal of Physics* **2010,** 12, (5), 055001.
63. Cipelletti, L.; Ramos, L.; Manley, S.; Pitard, E.; Weitz, D. A.; Pashkovski, E. E.; Johansson, M. Universal non-diffusive slow dynamics in aging soft matter. *Faraday Discuss.* **2003,** 123, (0), 237-251.
64. Bouchaud, J.-P.; Pitard, E. Anomalous dynamical light scattering in soft glassy gels. *The European Physical Journal E* **2001,** 6, (3), 231-236.
65. Hoshino, T.; Murakami, D.; Tanaka, Y.; Takata, M.; Jinnai, H.; Takahara, A. Dynamical crossover between hyperdiffusion and subdiffusion of polymer-grafted nanoparticles in a polymer matrix. *Physical Review E* **2013,** 88, (3), 032602.
66. Vallee, A.; Besner, S.; Prudhomme, J. COMPARATIVE-STUDY OF POLY(ETHYLENE OXIDE) ELECTROLYTES MADE WITH LIN(CF3SO2)2, LICF3SO3 AND LICLO4 - THERMAL-PROPERTIES AND CONDUCTIVITY BEHAVIOR. *Electrochim. Acta* **1992,** 37, (9), 1579-1583.
67. Marzantowicz, M.; Krok, F.; Dygas, J. R.; Florjanczyk, Z.; Zygadlo-Monikowska, E. The influence of phase segregation on properties of semicrystalline PEO: LiTFSI electrolytes. *Solid State Ionics* **2008,** 179, (27-32), 1670-1678.
68. Singh, M.; Odusanya, O.; Wilmes, G. M.; Eitouni, H. B.; Gomez, E. D.; Patel, A. J.; Chen, V. L.; Park, M. J.; Fragouli, P.; Iatrou, H.; Hadjichristidis, N.; Cookson, D.; Balsara, N. P. Effect of molecular weight on the mechanical and electrical properties of block copolymer electrolytes. *Macromolecules* **2007,** 40, (13), 4578-4585.

69. Gergesova, M.; Saprunov, I.; Emri, I. Closed-form solution for horizontal and vertical shiftings of viscoelastic material functions in frequency domain. *Rheol. Acta* **2016,** 55, (5), 351-364.
70. Rosedale, J. H.; Bates, F. S. RHEOLOGY OF ORDERED AND DISORDERED SYMMETRIC POLY(ETHYLENEPROPYLENE) POLY(ETHYLETHYLENE) DIBLOCK COPOLYMERS. *Macromolecules* **1990,** 23, (8), 2329-2338.
71. Riise, B. L.; Fredrickson, G. H.; Larson, R. G.; Pearson, D. S. Rheology and Shear-Induced Alignment of Lamellar Diblock and Triblock Copolymers. *Macromolecules* **1995,** 28, (23), 7653-7659.
72. Zhang, Y. M.; Wiesner, U. Rheology of lamellar polystyrene-block-polyisoprene diblock copolymers. *Macromol. Chem. Phys.* **1998,** 199, (9), 1771-1784.
73. Langela, M. Struktur und rheologische Eigenschaften von PS-PI und PS-PB Blockcopolymeren. PhD Thesis 2001, Johannes-Gutenberg-Universität Mainz, 2002.
74. Roland, C. M.; Casalini, R.; Paluch, M. Isochronal temperature–pressure superpositioning of the α-relaxation in type-A glass formers. *Chem. Phys. Lett.* **2003,** 367, (3), 259-264.
75. Matsumiya, Y.; Uno, A.; Watanabe, H.; Inoue, T.; Urakawa, O. Dielectric and Viscoelastic Investigation of Segmental Dynamics of Polystyrene above Glass Transition Temperature: Cooperative Sequence Length and Relaxation Mode Distribution. *Macromolecules* **2011,** 44, (11), 4355-4365.
76. Niedzwiedz, K.; Wischnewski, A.; Pyckhout-Hintzen, W.; Allgaier, J.; Richter, D.; Faraone, A. Chain dynamics and viscoelastic properties of poly(ethylene oxide). *Macromolecules* **2008,** 41, (13), 4866-4872.
77. Lutz, T. R.; He, Y. Y.; Ediger, M. D.; Cao, H. H.; Lin, G. X.; Jones, A. A. Rapid poly(ethylene oxide) segmental dynamics in blends with poly(methyl methacrylate). *Macromolecules* **2003,** 36, (5), 1724-1730.
78. Kossuth, M. B.; Morse, D. C.; Bates, F. S. Viscoelastic behavior of cubic phases in block copolymer melts. *J. Rheol.* **1999,** 43, (1), 167-196.
79. Fang, L.; Takahashi, Y.; Takano, A.; Matsushita, Y. A separation method of responses from large scale motions and chain relaxations for viscoelastic properties of symmetric poly(styrene-b-2-vinylpyridine)s in the ordered state. *Nihon Reoroji Gakkaishi* **2013,** 41, (2), 93-99.
80. Vogel, H. The temperature dependence law of the viscosity of fluids. *Physikalische Zeitschrift* **1921,** 22, 645-646.
81. Chintapalli, M.; Le, T. N.; Venkatesan, N. R.; Mackay, N. G.; Rojas, A. A.; Thelen, J. L.; Chen, X. C.; Devaux, D.; Balsara, N. P. Structure and Ionic Conductivity of Polystyrene-block-poly (ethylene oxide) Electrolytes in the High Salt Concentration Limit. *Macromolecules* **2016,** 49, (5), 1770-1780.
82. Henderson, W. A. Crystallization kinetics of glyme− LiX and PEO− LiX polymer electrolytes. *Macromolecules* **2007,** 40, (14), 4963-4971.
83. Fauteux, D.; McCabe, P. Thermal behavior of new polymer electrolytes. *Polymers for Advanced Technologies* **1995,** 6, (2), 83-90.
84. Lodge, T. P.; Dalvi, M. C. Mechanisms of Chain Diffusion in Lamellar Block-Copolymers. *Phys. Rev. Lett.* **1995,** 75, (4), 657-660.

85. Ryu, H. J.; Fortner, D. B.; Lee, S.; Ferebee, R.; De Graef, M.; Misichronis, K.; Avgeropoulos, A.; Bockstaller, M. R. Role of Grain Boundary Defects During Grain Coarsening of Lamellar Block Copolymers. *Macromolecules* **2013,** 46, (1), 204-215.
86. Tsarkova, L.; Knoll, A.; Magerle, R. Rapid Transitions between Defect Configurations in a Block Copolymer Melt. *Nano Lett.* **2006,** 6, (7), 1574-1577.
87. Hahm, J.; Sibener, S. J. Time-resolved atomic force microscopy imaging studies of asymmetric PS-b-PMMA ultrathin films: Dislocation and disclination transformations, defect mobility, and evolution of nanoscale morphology. *J. Chem. Phys.* **2001,** 114, (10), 4730-4740.
88. Sigel, R.; Pispas, S.; Vlassopoulos, D.; Hadjichristidis, N.; Fytas, G. Structural Relaxation of Dense Suspensions of Soft Giant Micelles. *Phys. Rev. Lett.* **1999,** 83, (22), 4666-4669.

For Table of Contents Only

Structural Dynamics of Strongly Segregated Block Copolymer Electrolytes

Onyekachi Oparaji,[a,b] Suresh Narayanan,[c] Alec Sandy,[c] Subramanian Ramakrishnan,[a,b] and Daniel Hallinan Jr.[a,b,*]